2014 Conductivity Anomaly , 21-28

Simulation of the electromagnetic fields induced by Tohoku tsunamis of 2011

Luolei Zhang, Hisashi Utada, Hisayoshi Shimizu, Kiyoshi Baba, and Takuto Maeda

Earthquake Research Institute, University of Tokyo, Yayoi 1-1-1, Bunkyo-ku, Tokyo, 113-0032, Japan

Abstract: The motion of seawater induces electromotive force of significant intensity due to Faraday's law, and resulting electromagnetic field can be recorded by instruments installed on land or at ocean bottom. However, a few studies were successfully simulating motionally induced electromagnetic (EM) fields by an exact and accurate application of Maxwell equations. We built an accurate scheme for numerical simulation to calculate EM fields due to ocean tidal flow, and compared the calculated magnetic field with that observed in response to the devastating Tohoku tsunami of 2011, to check the accuracy of the code. It shows that our results are in good agreement with observations. We also defined the motional impedance just as the case of ordinary magnetotellurics and showed that both calculated and observed impedances approximately indicate the phase velocity of the long wave as predicted by a simple theory.

Keywords: 3-D forward calculation, tsunami, magnetic field, magnetotellurics

Introduction

The motion of seawater induces electromotive force of significant intensity [*Sanford*, 1971] due to Faraday's law, and the resulting electromagnetic (EM) field can be recorded on land, ocean bottom, and in space [*Tyler et al.*, 2003; *Manoj et al.*, 2011; *Toh et al.*, 2011]. However, only a few studies were successfully simulating tsunami induced EM fields by an exact and accurate application of Maxwell equations that is essential for a quantitative interpretation to get geophysical information from observations of related EM signals.

There are a number of observations of such EM fields that were caused by the devastating Tohoku tsunami in March 2011, not only from land observatories but also from the seafloor site (Figure 1). We propose an accurate scheme for a numerical simulation of tsunami-induced EM field variations at these sites. We adopt a kinematic approach to calculate the fields in which the source electric current is calculated from a flow model obtained by a tsunami simulation. We apply a 3-D EM induction code in a Cartesian coordinate system with a heterogeneous source term, which is based on the modified iterative dissipative method (MIDM) [*Singer*, 1995; *Pankratov et al.*, 1995; *Zhang et al.*, 2012]. By using the developed code, we examine how the observed signals are explained by the applied model.

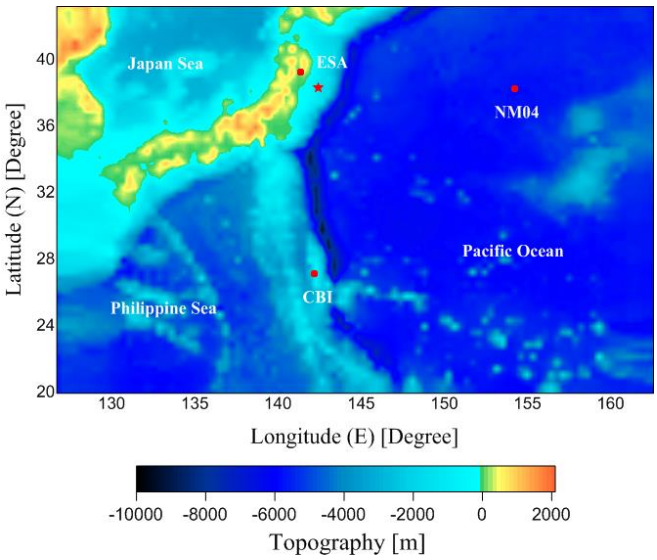

Fig. 1 Topographic map with positions of observation points (ESA, CBI, and NM04). The epicenter of the 2011 Tohoku Earthquake is shown by a red star.

Simulation Method

For a quasi-stationary EM field (i.e., the displacement currents are ignored), assuming a harmonic time dependence of $e^{-i\omega t}$, where $i = \sqrt{(-1)}$ and ω is the angular frequency, Maxwell equations can be written as follows:

$$\begin{aligned} \frac{1}{\mu_0}\nabla\times\mathbf{B}(\mathbf{r};\omega) &= \sigma(\mathbf{r})\mathbf{E}(\mathbf{r};\omega)+\mathbf{J}^{ext}(\mathbf{r};\omega) \\ \nabla\times\mathbf{E}(\mathbf{r};\omega) &= \mathrm{i}\omega\mathbf{B}(\mathbf{r};\omega) \end{aligned} \tag{1}$$

In these equations, **E** and **B** are the electric and magnetic fields, respectively, σ and μ_0 denote the electrical conductivity and magnetic permeability, respectively ($\mu_0 = 4\pi \times 10^{-7}$ H/m is the magnetic permeability of free space), and $\mathbf{J}^{ext}$ is the extrinsic source current.

For a conductor, such as seawater, moving in the ambient geomagnetic field, the extrinsic current $\mathbf{J}^{ext}$ can be calculated as follows:

$$\mathbf{J}^{ext}(\mathbf{r},\omega)=\sigma_{\mathrm{w}}(\mathbf{r})\cdot(\mathbf{v}(\mathbf{r},\omega)\times\mathbf{B}_0(\mathbf{r})) \tag{2}$$

where σ_{w} is the electrical conductivity of the moving conductor (the seawater conductivity in the present case is assumed to be constant at 3.2 S/m), **v** is the vector of the fluid velocity, and $\mathbf{B}_0$ is the vector of the ambient magnetic field that can be approximated by the International Geomagnetic Reference Field (IGRF) at each point. The time variation in $\mathbf{B}_0$ is small, so $\mathbf{B}_0$ is assumed to be time-independent.

Source Current and Model Construction

The extrinsic source current distribution is predicted from the flow data (a vector of the depth-integrated velocity) calculated by a tsunami simulation in two-dimensional (2-D) Cartesian

coordinates in the x-y plane based on the linear long-wave theory [*Maeda et al.*, 2011]. Velocity data (a vector of the depth-integrated velocity divided by the water depth) from the tsunami simulation sampled at every minute for 180 min after the origin time of the Tohoku earthquake were transformed to the frequency domain at each grid point for the MIDM solver. The MIDM solver provides a frequency domain solution of Maxwell equations at each observation site. The frequency domain solutions are then transformed back to the time domain to be compared with observations.

For the model construction, we refer to topographic map ETOPO-1 (from the U.S. National Oceanic and Atmospheric Administration's National Geophysical Data Center) of the seafloor. Above the seafloor, we assume a constant seawater conductivity of 3.2 S/m. Under the seafloor, we assumed a sedimentary layer with a constant thickness of 1 km. Below the sediment layer, we assumed at every grid point a 1-D profile based on the results obtained by *Baba et al.* [2010] for either the Northwest Pacific (in the case of modeling ESA and NM04) or the Philippine Sea (in the case of modeling CBI), if the sea depth is greater than 3000 m. If the sea depth is less than 3000 m (except land), we assumed the conductivity below the sediment layer to be constant at 0.001 S/m down to the depth of 30 km. Thus, for this case study, we can get a simple 3-D electrical conductivity structure with only lateral heterogeneity due to undulating seafloor topography and land-sea distribution (Figure 2).

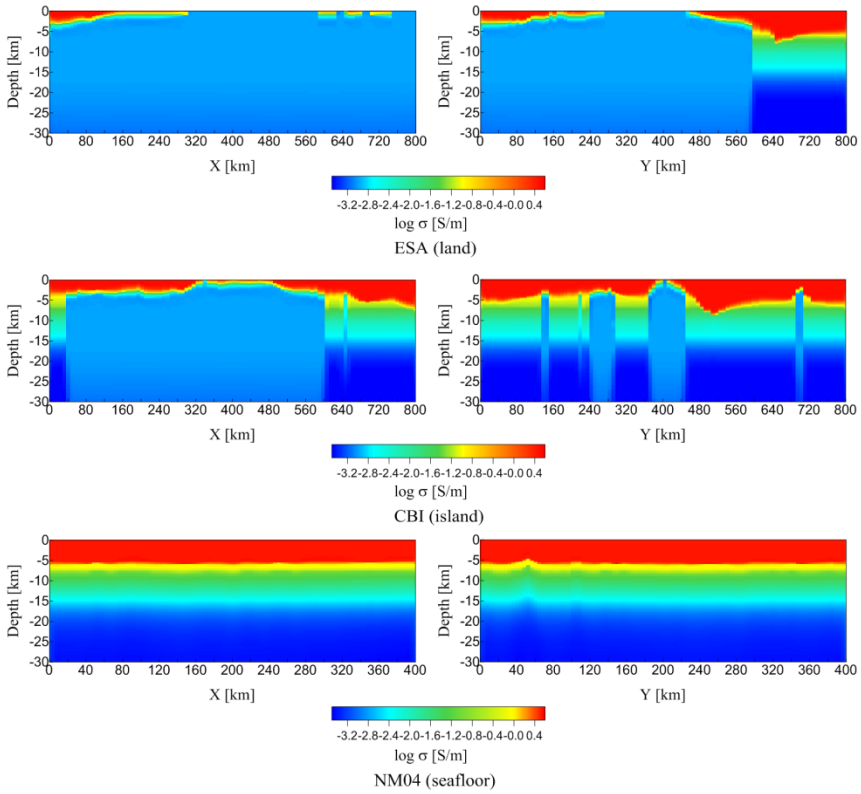

Fig. 2 N-S (right) and E-W (left) cross-sections of the electrical conductivity models for ESA (top), CBI (middle) and NM04 (bottom) used in this study.

Simulation Method

ESA (Land site)

First, we show the simulation result for the magnetic field at ESA in the Tohoku district. Figure 3 compares vertical components of the magnetic field (black), calculated by the same manner as in *Utada et al.* [2011], i.e., applying the Biot-Savart law (blue) and calculated by the present method. As reported, there was a sudden depression of the observed field for 10 min after the earthquake origin time at this site. Although the present result shows a tendency of some depression, the amplitude is much smaller than the observed amplitude. Calculation by the Biot-Savart law gives a slightly larger amplitude, but it is still smaller than the observation result. The relation between these two calculations looks reasonable, because the EM induction will reduce the magnetic effect from the electric current. The smaller amplitude compared to the observation may indicate that the tsunami simulation applied in this study underestimated the tsunami flux in this area (the northern part of the Tohoku district).

The significant variation in the observed field starting at about 10 min after the origin time is probably caused by the ionospheric disturbance [e.g., *Tsugawa et al.*, 2011] and therefore should not be compared with the present EM simulation result.

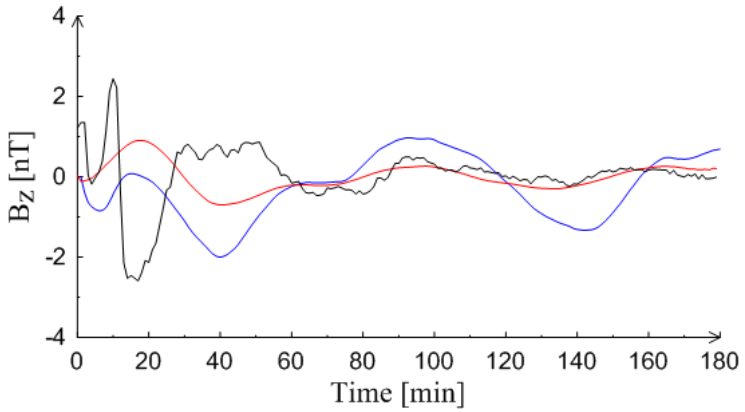

Fig. 3 The vertical component of the simulated magnetic field, B_z, at ESA. Time variations by using the Biot-Savart law (blue), by 3-D simulation (red), and by observation (black) are shown against the elapsed time

CBI (Island Site)

Figure 4 shows the results for the island site, CBI. In Figure 4a, the vertical component calculated using the Biot-Savart law and that of the field from the resistive uniform half-space (10^{-6} S/m) were compared with the observation results. We can see the qualitative agreement regarding the arrival time, but the model results are greater in amplitude than the observation results. However, as shown in Figure 4b, the total vertical magnetic field B_z from the 3-D simulation shows reasonable agreement with the observation, with only a slightly smaller amplitude than the observed amplitude. There is also a small time shift between the simulation result and the observation. We believe these discrepancies are caused by the inaccuracy of the tsunami simulation in the Cartesian coordinate system (the effect of the sphericity of Earth is significant).

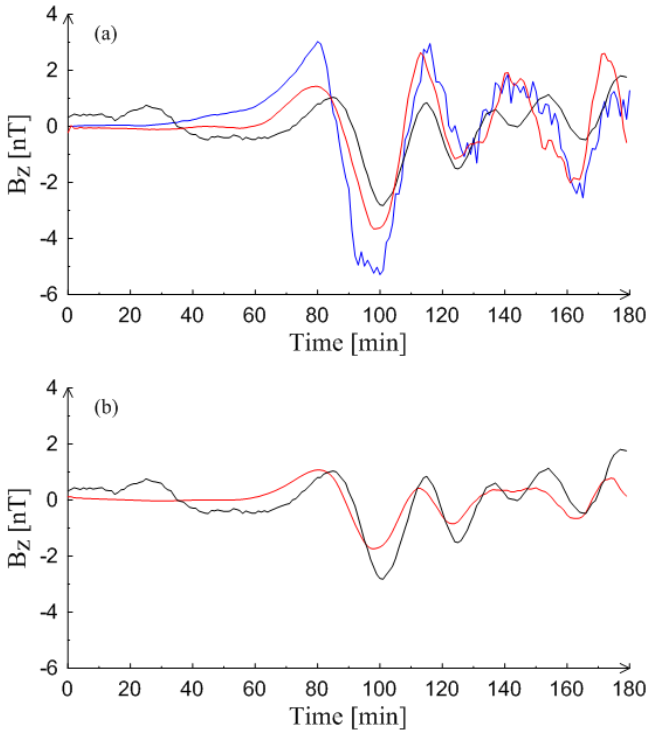

Fig. 4 Various comparisons of the vertical component B_z of the magnetic field at the island site, CBI. (a) Result obtained using the Biot-Savart law (blue), the resistive uniform half-space (red), and by observation (black). (b) Simulated field (red) from all source current elements and observation (black).

NM04 (Seafloor Site)

Figure 5 shows a comparison in time series of the simulation results (red) and the observations (black) for seafloor site NM04. Figure 5a shows the tsunami height calculated by the tsunami simulation. Figures 5b–d compare the eastward component, B_y, and the vertical component, B_z, of the magnetic field, and the northward component of the electric field E_x, respectively, which are the dominant components in the present case. Reasonable agreement is seen between the models and observations, especially for the main phase.

There is a slight difference in the arrival time of the tsunami-induced EM field: the simulated field arrives earlier by about 5 min than the observed field, which we suspect is caused by the different distances between points on the true spherical Earth and the flat version of Earth that we used. The simulation results do not reproduce the continuous fluctuation following the main phase that is clearly seen in observation. This fluctuation is due to the high-frequency dispersion of the tsunami [e.g., *Saito and Furumura*, 2009], which was not considered in the present tsunami simulation based on the linear long-wave approximation.

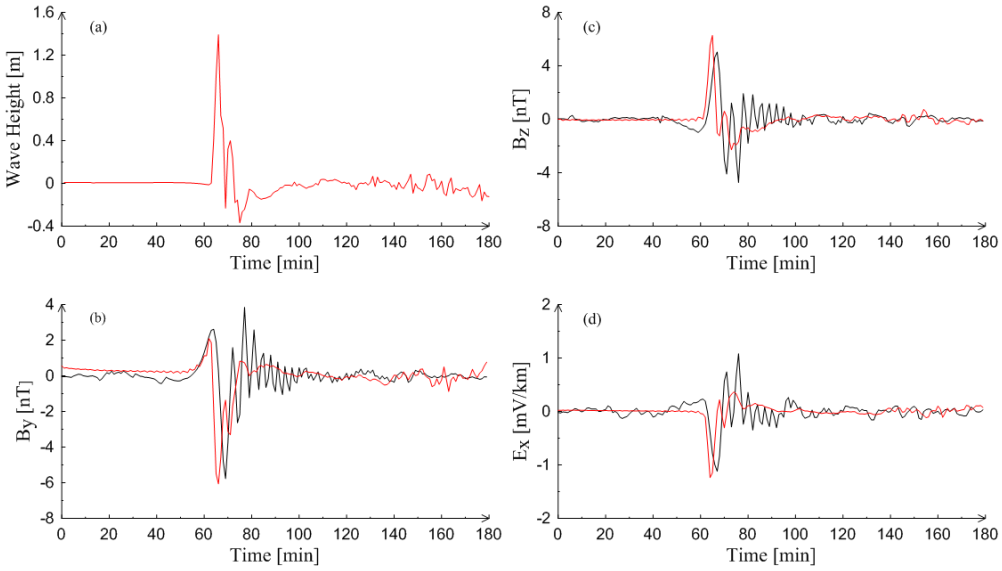

Fig. 5 Simulation results (red) and observations (black) at the seafloor site NM04. Shown are (a) wave height, (b) horizontal magnetic field B_y, (c) vertical magnetic field B_z, and (d) horizontal electrical field E_x.

Motional magnetotellurics

If a tsunami passes a seafloor MT observation, we have simultaneous record of electromagnetic field. Then a treatment of EM field data similar to the magnetotelluric processing can be applied. We also define the impendence and tipper as:

$$Z_{tr}(\mathbf{r};\omega) = \frac{E_t(\mathbf{r};\omega)}{B_r(\mathbf{r};\omega)}, M_{zr}(\mathbf{r};\omega) = \frac{B_z(\mathbf{r};\omega)}{B_r(\mathbf{r};\omega)} \tag{3}$$

where suffixes t , r and z stand for the transverse, radial and vertical directions relative to the tsunami propagation direction. For a 1-D long wave propagating in y direction, they can be related as,

$$Z_{tr}(\mathbf{r};\omega) = \frac{\omega}{k} M_{zr}(\mathbf{r};\omega) \tag{4}$$

where k is the wave number.

We calculate the amplitude and phase of Z_{xy} and M_{zy}•k/ω from the observations (Figure 6) and simulation results (Figure 7). We compared the amplitude and phase of calculated impendence and tipper with those calculated by half spaces with uniform resistivity of 1 Ω.m (blue line), 10 Ω.m (green line) and 100 Ω.m (red line). We notice that the motional impedance and tipper can be an easy indicator for exploring the crust and mantle but useful only at longer periods. When the period is shorter, the response functions only indicate the mean ocean depth, because the impedance amplitude approaches to the phase velocity of the long wave. All curves of Z_{xy} and M_{zy}•k/ω (black line) from simulations and observations are rather in good agreement, which means the sea bed structure is close to 1-D.

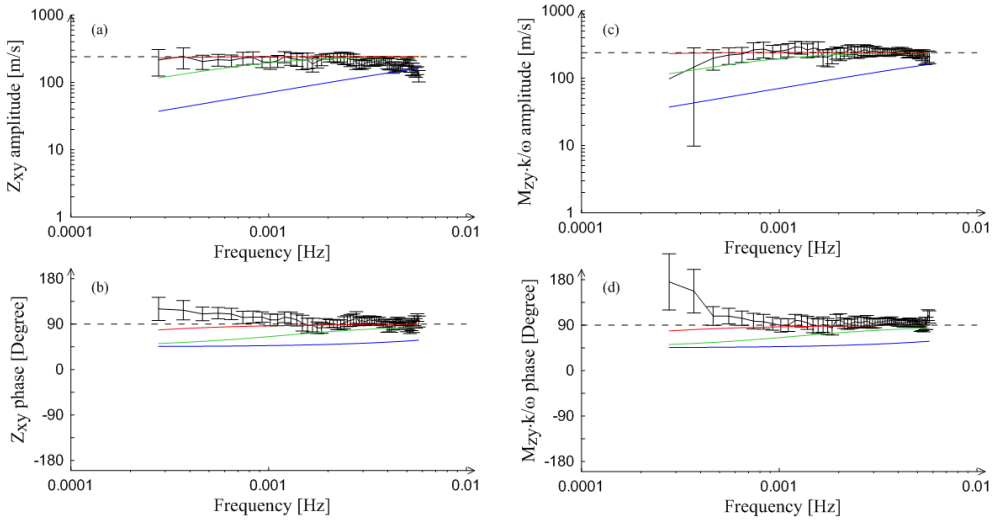

Fig. 6 Motional impedance, Z_{xy}, and motional tipper, M_{zy}, at NM04 obtained from observation (black) and from calculation by one-dimensional assumption with uniform sub-bottom conductivity of 0.01 (red), 0.1 (green), and 1 (blue) S/m. The approximate long wave velocity and the phase of 90 degree are given by the dashed lines.

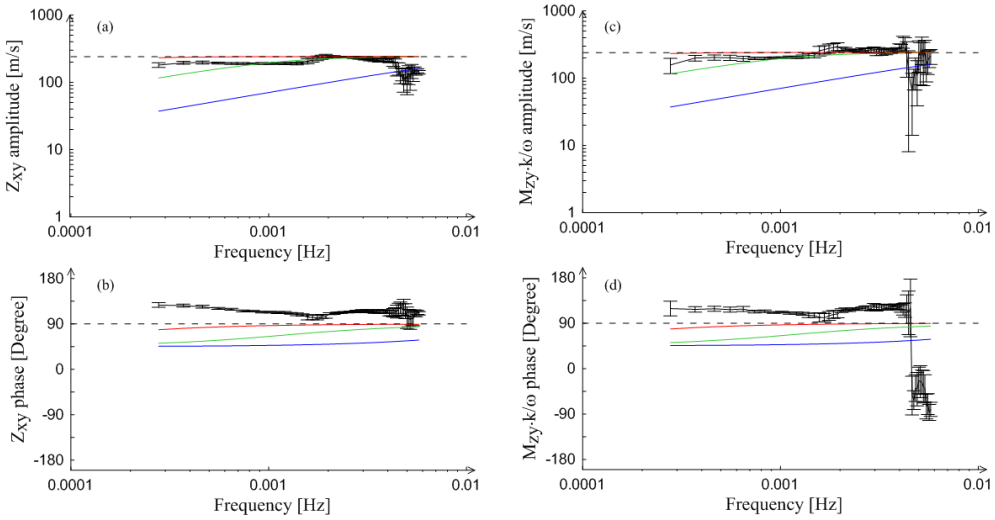

Fig. 7 Motional impedance, Z_{xy}, and motional tipper, M_{zy}, at NM04 obtained from the 3-D simulation (black) and from calculation in one-dimensional assumption with uniform sub-bottom conductivity of 0.01 (red), 0.1 (green), and 1 (blue) S/m. The approximate long wave velocity and the phase of 90 degree are given by the dashed lines.

Conclusions

We applied a 3-D EM induction code in a Cartesian coordinate system based on the MIDM with the heterogeneous source current term obtained from a tsunami simulation. The EM simulation results can be summarized as follows: The simulated EM fields showed reasonable agreement with observations on land, on an island, and on the seafloor. Motional impedance and tipper can be an easy indicator for exploring the crust and mantle but are useful only for longer periods. With decreasing periods, these response functions tend to indicate only the mean ocean depth (the phase velocity of a long wave).

References

Baba, K., H. Utada, T. Goto, T. Kasaya, H. Shimizu, and N. Tada (2010), Electrical conductivity imaging of the Philippine Sea upper mantle using seafloor magnetotelluric data, *Phys. Earth Planet. Int.*, *183*(1–2), 44-62, doi:10.1016/j.pepi.2010.09.010.

Maeda, T., T. Furumura, S. Sakai, and M. Shinohara (2011), Significant tsunami observed at ocean-bottom pressure gauges during the 2011 off the Pacific coast of Tohoku earthquake, *Earth Planets Space*, *63*, 803–808, doi:10.5047/eps.2011.06.005.

Manoj, C., S. Maus, and A. Chulliat (2011), Observation of magnetic fields generated by tsunamis, *Eos Trans. AGU*, *92*(2), 13–14, doi:10.1029/2011EO020002.

Pankratov, O.V., D.B. Avdeyev, and A.V. Kuvshinov (1995), EM field scattering in a heterogeneous Earth: a solution to the forward problem, *Physics of the Solid Earth , English Translation*, *31*(3), 201–209.

Saito, T., and T. Furumura (2009), Three-dimensional simulation of tsunami generation and propagation: application to intraplate events, *J. Geophys. Res.*, *114*(B2), B02307, doi:10.1029/2007JB005523.

Sanford, T.B. (1971), Motionally induced electric and magnetic fields in the sea, *J. Geophys. Res.*, *76*(15), 3476–3492, doi:10.1029/JC076i015p03476.

Singer, B.S. (1995), Method for solution of Maxwell's equations in non-uniform media, *Geophys. J. Int.*, *120*(3), 590–598, doi:10.1111/j.1365-246X.1995.tb01841.x.

Toh, H., K. Satake, Y. Hamano, Y. Fujii, and T. Goto (2011), Tsunami signals from the 2006 and 2007 Kuril earthquakes detected at a seafloor geomagnetic observatory, *J. Geophys. Res.*, *116*(B2), B02104, doi:10.1029/2010JB007873.

Tsugawa, T., A. Saito, Y. Otsuka, M. Nishioka, T. Maruyama, H. Kato, T. Nagatsuma, and K. Murata (2011), Ionospheric disturbances detected by GPS total electron content observation after the 2011 off the Pacific coast of Tohoku Earthquake, *Earth Planets Space*, *63*, 875–879, doi:10.5047/eps.2011.06.035.

Tyler, R.H., S. Maus, and H. Luhr (2003), Satellite observations of magnetic fields due to ocean tidal flow, *Science*, *299*(5604), 239–241-Doi:10.1126/science.1078074.

Utada, H., H. Shimizu, T. Ogawa, T. Maeda, T. Furumura, T. Yamamoto, N. Yamazaki, Y. Yoshitake, and S. Nagamachi, (2011), Geomagnetic field changes in response to the 2011 off the Pacific Coast of Tohoku Earthquake and Tsunami, *Earth Planet. Sci. Lett.*, *311*(1-2), 11–27, doi:10.1016/j.epsl.2011.09.036.

Zhang, L., T. Koyama, H. Utada, P. Yu, and J. Wang (2012), A regularized three-dimensional magnetotelluric inversion with a minimum gradient constrain, *Geophys. J. Int.*, *189*(1), 296–316, doi: 10.1111/j.1365-246X.2012.05379.x.